Calculation of Solid−Liquid Work of Adhesion Patterns from Combining Rules for Intermolecular Potentials

Junfeng Zhang and Daniel Y. Kwok*

Nanoscale Technology and Engineering Laboratory,‡ Department of Mechanical Engineering, University of Alberta, Edmonton, Alberta T6G 2G8, Canada

Received: August 3, 2002; In Final Form: October 2, 2002

The thermodynamic work of solid−liquid adhesion is a well-defined property. Their phenomenological patterns relating to surface tensions, however, have not been well-characterized. We employed a hard sphere model to determine the solid−liquid work of adhesion patterns from a mean-field theory through calculations of the liquid−vapor, solid−vapor, and solid−liquid interfacial tensions. By plotting the work of adhesion with the liquid−vapor interfacial tension, we constructed curves that appear to behave in a very regular manner for a variety of combining rules; the curves shift regularly when we increase the strength of solid−solid interaction and hence the solid−vapor surface tension. Contact angle patterns were also constructed via Young's equation. We found that, except Berthelot's rule, the (9:3), Steele, and (12:6) combining rules yield essentially similar adhesion patterns. The regularity of the patterns is remarkable and in reasonable agreement with recent experimental findings. We have shown that macroscopic experimental adhesion and contact angle patterns can, in principle, be reproduced from consideration of only intermolecular forces. The exact patterns depend on the choice of the combining rules.

I. Introduction

Macroscopic contact angle phenomena have long been the interest of scientists and engineers because of the possibility to relate the nonmeasurable thermodynamic property, solid surface tension, to contact angle through Young's equation:

$$\gamma_{lv} \cos \theta_Y = \gamma_{sv} - \gamma_{sl} \tag{1}$$

where γ_{lv}, γ_{sv}, and γ_{sl} are the surface tensions of the liquid−vapor, solid−vapor, and solid−liquid interfaces, respectively, and θ_Y is the Young contact angle, that is, a contact angle that can be inserted into Young's equation. Contact angle measurement is easily performed by establishing the tangent (angle) of a liquid drop with a solid surface at the base. The attractiveness of using contact angles θ to estimate the solid−vapor and solid−liquid interfacial tensions is due to the relative ease with which contact angles can be measured on suitably prepared solid surfaces. It is, however, apparent in the literature that this seeming simplicity for the interpretation of solid surface tensions can be misleading.[1,2]

An alternative approach to understand contact angles is based on combining rules for the intermolecular potential. In general, a number of combining rules have been proposed as attempts for a better representation of solid−liquid interactions from solid−solid and liquid−liquid interactions. However, the validity of these existing combining rules for solid−liquid systems often lacks experimental support. This is due to the difficulties involved in estimating the operative solid−liquid interactions. One attractive alternative is by means of the thermodynamic free energy of adhesion via wetting as recently accomplished.[3]

More recently, Kwok et al.[3−5] published contact angle and adhesion patterns for a number of low-energy solid surfaces. The regularity of their patterns is indeed striking. This study explores whether such macroscopic adhesion patterns could be reproduced by consideration of only intermolecular interaction forces between the liquid−vapor, solid−liquid, and solid−vapor interfaces. A generalized van der Waals theory will be employed to model unlike molecular interactions from a mean-field approximation for calculations of γ_{lv}, γ_{sv}, and γ_{sl}. From these calculated interfacial tensions, we examine the adhesion and contact angle patterns for a variety of established combining rules. Our aim is to test existing combining rules for solid−liquid intermolecular potential and, as a second objective, to construct adhesion patterns and compare them with experimental results.

II. Theory

A. Combining Rules. In the theory of molecular interactions and the theory of mixtures, combining rules are used to evaluate the parameters of unlike-pair interactions in terms of those of the like-pair interactions.[6−15] As with many other combining rules, the Berthelot rule[16]

$$\epsilon_{ij} = \sqrt{\epsilon_{ii}\epsilon_{jj}} \tag{2}$$

is a useful approximation but does not provide a secure basis for the understanding of unlike-pair interactions; ϵ_{ij} is the potential energy parameter (well depth) of unlike-pair interactions; ϵ_{ii} and ϵ_{jj} are for like-pair interactions.

From the London theory of dispersion forces, the attraction potential ϕ_{ij} between a pair of unlike molecules i and j is given by

$$\phi_{ij} = -\frac{3}{2}\frac{I_i I_j}{I_i + I_j}\frac{\alpha_i \alpha_j}{r_{ij}^6} \tag{3}$$

* To whom correspondence should be addressed. Electronic address: daniel.y.kwok@ualberta.ca.
‡ URL: http://nanotech.ualberta.ca.

10.1021/jp026676t CCC: $22.00
Published on Web 10/31/2002

where I is the ionization potential and α the polarizability. For like molecules, this term becomes

$$\phi_i = -\frac{3}{4}\frac{I_i {\alpha_i}^2}{{r_i}^6} \tag{4}$$

The total intermolecular potential $V(r_i)$ expressed by the (12:6) Lennard-Jones potential is in the form

$$V(r_i) = 4\epsilon_{ii}((\sigma_i/r_i)^{12} - (\sigma_i/r_i)^6) \tag{5}$$

where σ is the collision diameter. The attractive potentials in eqs 4 and 5 can be equated to give

$$\frac{3}{4} I_i {\alpha_i}^2 = 4\epsilon_{ii}{\sigma_i}^6 \tag{6}$$

Equation 6 can be used to derive α_i and α_j; substituting these quantities into eq 3 yields

$$\phi_{ij} = -\frac{2\sqrt{I_i I_j}}{I_i + I_j}\frac{4{\sigma_i}^3{\sigma_j}^3}{{r_{ij}}^6}\sqrt{\epsilon_{ii}\epsilon_{jj}} \tag{7}$$

If we write ϕ_{ij} in the form $-4\epsilon_{ij}{\sigma_{ij}}^6/{r_{ij}}^6$ such that $\sigma_{ij} = (\sigma_i + \sigma_j)/2$, the energy parameter for two unlike molecules can be expressed as

$$\epsilon_{ij} = \left(\frac{2\sqrt{I_i I_j}}{I_i + I_j}\right)\left(\frac{4\sigma_i/\sigma_j}{(1 + \sigma_i/\sigma_j)^2}\right)^3\sqrt{\epsilon_{ii}\epsilon_{jj}} \tag{8}$$

This forms the basis of the so-called combining rules for intermolecular potential. The above expression for ϵ_{ij} can be simplified: when $I_i = I_j$, the first term of eq 8 becomes unity; when $\sigma_i = \sigma_j$, the second factor becomes unity. When both conditions are met, we obtain the well-known Berthelot rule, that is, eq 2.

For the interactions between two very dissimilar types of molecules or materials for which there is an apparent difference between ϵ_{ii} and ϵ_{jj}, it is clear that the Berthelot rule cannot describe the behavior adequately. It has been demonstrated[17,18] that the Berthelot geometric mean combining rule generally overestimates the strength of the unlike-pair interactions, that is, the geometric mean value is too large an estimate. In general, the differences in the ionization potential are not large, that is, $I_i \approx I_j$; thus, the most serious error comes from the difference in the collision diameters σ for unlike molecular interactions.

For solid−liquid systems in general, the minimum of the solid−liquid interaction potential, ϵ_{sl}, is often expressed in the following manner:[6,9,11]

$$\epsilon_{sl} = g(\sigma_l/\sigma_s)\sqrt{\epsilon_{ss}\epsilon_{ll}} \tag{9}$$

where $g(\sigma_l/\sigma_s)$ is a function of σ_l and σ_s; they are, respectively, the collision diameters for the liquid and solid molecules; ϵ_{ss} and ϵ_{ll} are, respectively, the minima in the solid−solid and liquid−liquid potentials. Several other forms for the explicit function of $g(\sigma_l/\sigma_s)$ have been suggested. For example, by comparing ϵ_{sl} with the minimum in the (9:3) Lennard-Jones potential, one obtains an explicit function as

$$g(\sigma_l/\sigma_s) = \frac{1}{8}\left(1 + \frac{\sigma_l}{\sigma_s}\right)^3 \tag{10}$$

and the (9:3) combining rule becomes

$$\epsilon_{sl} = \frac{1}{8}\left(1 + \frac{\sigma_l}{\sigma_s}\right)^3\sqrt{\epsilon_{ss}\epsilon_{ll}} \tag{11}$$

An alternative function in the form of

$$g(\sigma_l/\sigma_s) = \frac{1}{4}\left(1 + \frac{\sigma_l}{\sigma_s}\right)^2 \tag{12}$$

has been investigated by Steele[19] and others,[20] suggesting a different combining rule as

$$\epsilon_{sl} = \frac{1}{4}\left(1 + \frac{\sigma_l}{\sigma_s}\right)^2\sqrt{\epsilon_{ss}\epsilon_{ll}} \tag{13}$$

For comparison purpose, we label eq 13 as the Steele combining rule in this paper. Further, from the (12:6) Lennard-Jones potential, eq 8 implies an explicit function

$$g(\sigma_l/\sigma_s) = \left(\frac{4\sigma_l/\sigma_s}{(1 + \sigma_l/\sigma_s)^2}\right)^3 \tag{14}$$

resulting in a (12:6) combining rule as

$$\epsilon_{sl} = \left(\frac{4\sigma_l/\sigma_s}{(1 + \sigma_l/\sigma_s)^2}\right)^3\sqrt{\epsilon_{ss}\epsilon_{ll}} \tag{15}$$

These are numerous attempts for a better representation of solid−liquid interactions from solid−solid and liquid−liquid interactions. In general, these functions are normalized such that $g(\sigma_l/\sigma_s) = 1$ when $\sigma_l = \sigma_s$; they revert to the Berthelot geometric mean combining rule eq 2 when $g(\sigma_l/\sigma_s) = 1$. Nevertheless, adequate representation of unlike solid−liquid interactions from like pairs is rare, and their validity for solid−liquid systems lacks experimental support. These commonly cited combining rules will be used in our calculations of the thermodynamic adhesion patterns from γ_{lv}, γ_{sv}, and γ_{sl}.

B. Contact Angles and Adhesion. Thermodynamically, a relation of the free energy of adhesion per unit area of a solid−liquid pair is equal to the work, W_{sl}, required to separate unit area of the solid−liquid interface:[21]

$$W_{sl} = \gamma_{lv} + \gamma_{sv} - \gamma_{sl} \tag{16}$$

Because the free energy is directly proportional to the energy parameter,[22,23] that is, $W \propto \epsilon$, the Berthelot geometric mean combining rule (eq 2) for the free energy of adhesion, W_{sl}, can be approximated in terms of the free energy of cohesion of the solid, W_{ss} and that of the liquid, W_{ll},[16,22−24]

$$W_{sl} = \sqrt{W_{ll}W_{ss}} \tag{17}$$

By the definitions $W_{ll} = 2\gamma_{lv}$ and $W_{ss} = 2\gamma_{sv}$, eq 17 becomes

$$W_{sl} = 2\sqrt{\gamma_{lv}\gamma_{sv}} \tag{18}$$

Experimentally one can in principle obtain the free energy of adhesion W_{sl} through contact angles via Young's equation (eq 1). Combining eqs 1 and 16 eliminates γ_{sv} and γ_{sl} and yields a relation of W_{sl} as a function of only γ_{lv} and θ_Y:

$$W_{sl} = \gamma_{lv}(1 + \cos\theta_Y) \tag{19}$$

Thus, in addition to eq 16, adhesion patterns can also be obtained from experimental contact angles, that is, contact angles of different liquids on one and the same solid surface can be employed to study a systematic effect of changing γ_{lv} on W_{sl} through θ_Y.

C. Calculation of Interfacial Tensions and Contact Angles. We employ a mean-field approximation here to calculate numerically the three interfacial tensions from molecular interactions. In our simple van der Waals model, the fluid molecules are idealized as hard spheres interacting with each other through a potential $\phi_{ff}(r)$, where r is a distance between two interacting molecules. A Carnahan−Starling model[10,25,26] is adopted as the hard sphere reference system. For a planer interface formed by a liquid and its vapor, each of which occupies a semi-infinite space, $z > 0$ and $z < 0$, respectively, and the surface tension is given by[11,25]

$$\gamma_{lv} = \min_{\rho} \int_{-\infty}^{+\infty} dz \left\{ F[\rho(z)] + \frac{1}{2}\rho(z) \int_{-\infty}^{+\infty} dz' \bar{\phi}_{ff}(z' - z)[\rho(z') - \rho(z)] \right\} \quad (20)$$

Here, the minimum is taken over all possible density profiles $\rho(z)$ and F is the excess free energy; $\bar{\phi}_{ff}$ represents the interaction potential that has been integrated over the whole $x'y'$ plane. For the solid−fluid (i.e., a solid−liquid or a solid−vapor) interface, the solid is modeled as a semi-infinite impenetrable wall occupying the domain of $z < 0$ and exerting an attraction potential $V(z)$ to the fluid molecule at a distance z from the solid surface. The interfacial tension of such an interface can be obtained from

$$\gamma_{sf} = \gamma_s + \min_{\rho} \int_{0}^{+\infty} dz \left\{ F[\rho(z)] + \rho(z)V(z) + \frac{1}{2}\rho(z) \int_{0}^{+\infty} dz' \bar{\phi}_{ff}(z' - z)[\rho(z') - \rho(z)] - \frac{1}{2}\rho^2(z) \int_{-\infty}^{0} dz' \bar{\phi}_{ff}(z' - z) \right\} \quad (21)$$

where γ_s is the solid−vacuum surface tension, a constant that exists in the calculations of γ_{sv} and γ_{sl}. This constant (γ_s) will be canceled out in the calculations of the work of adhesion and contact angles via eq 16 and Young's equation (eq 1), respectively; it has no impact on the implication of our results because we are interested only in the difference between γ_{sv} and γ_{sl}. Considering a solid with molecules interacting with fluid molecules through a potential $\phi_{sf}(r)$, we obtain easily the intermolecular potential $V(z)$ by integrating $\phi_{sf}(r)$ over the solid domain. We wish to point out that the above equations for γ_{lv} and γ_{sf} (eqs 20 and 21) are identical to those reported in ref 11, although the form of equations are different.

To carry out the calculations of interfacial tensions and hence the contact angles, a given interaction potential is required. Here, we assume a (12:6) Lennard-Jones potential model and consider only the attraction part. It should be addressed that the Lennard-Jones potential function requires knowledge of two parameters: the potential strength ϵ and the collision diameter σ. The potential strength ϵ_{sf} for $\phi_{sf}(r)$ is obtained from the fluid, ϵ_{ff}, and solid, ϵ_{ss}, potential strengths via a combining rule, such as those given by eqs 11, 13, or 15. Once all interfacial tensions (γ_{lv}, γ_{sv}, and γ_{sl}) are calculated, eq 16 is used to determine the work of adhesion W_{sl}; alternatively, eq 19 can be used to determine W_{sl} from γ_{lv} and θ_Y through Young's equation.

TABLE 1: Comparison between the Calculated, γ_{lv}^{cal}, and Experimental, γ_{lv}^{exp}, Liquid−Vapor Surface Tensions (mJ/m^2)[a]

liquid	γ_{lv}^{exp}	γ_{lv}^{cal}	liquid	γ_{lv}^{exp}	γ_{lv}^{cal}
CH_3Cl	16.20[b]	13.72	hexadecane	27.76	17.68
pentane	16.65	13.07	CH_2Cl_2	27.84[b]	24.69
hexane	18.13	15.00	benzene	28.88[b]	26.04
methylamine	19.89[b]	16.98	*trans*-decalin	29.50	26.15
methanol	22.30	29.28	*cis*-decalin	31.65	26.77
decane	23.43	17.83	CS_2	32.32[b]	33.44
ethyl acetate	23.97[b]	18.85	chlorobenzene	33.59[b]	30.95
acetone	24.02[b]	20.14	bromobenzene	35.82[b]	34.15
ethyl methyl ketone	24.52[b]	21.29	iodobenzene	39.27[b]	38.38
methyl acetate	25.10	19.98	aniline	42.67[b]	38.55
dodecane	25.44	18.08	diethylene glycol	45.04	36.01
tetradecane	26.55	16.82	ethylene glycol	47.99	45.72
CCl_4	27.04[b]	24.29	glycerol	63.11	50.32
fluorobenzene	27.26[b]	24.59	hydrazine	67.60[b]	71.81
$CHCl_3$	27.32[b]	25.01	water	72.75	92.92

[a] Experimental values were obtained from ref 5 at 21 °C. [b] From ref 27 measured at 20 °C.

As mentioned above, the calculation of liquid surface tension, γ_{lv}, requires two parameters, ϵ_{ff} and σ_f, which can be related to the critical temperature T_c and pressure P_c of the liquid by the Carnahan−Starling model[10,25] in the following expressions:

$$kT_c = 0.180\ 16\alpha/\sigma_f^3$$
$$P_c = 0.016\ 11\alpha/\sigma_f^6 \quad (22)$$

where k is the Boltzmann constant and α is the van der Waals parameter given by

$$\alpha = -\frac{1}{2}\int \phi_{ff}(r)\, dr \quad (23)$$

The densities of the liquid, ρ_l, and vapor, ρ_f, were obtained by requiring the liquid and vapor to be in coexistence at a given temperature T.[10,25] In our calculations, we have selected 30 liquids of different molecular structures and have assumed $T =$ 21 °C, $\sigma_s = 10$ Å, and $\rho_s = 10^{27}$ molecules/m^3 for the solid surface.

III. Results and Discussion

A. Liquid−Vapor Surface Tensions. We show in Table 1 the calculated liquid surface tensions for the 30 liquids selected. In most cases, the differences between the calculated and experimental liquid−vapor surface tensions are less than 10−20%. The largest discrepancy comes from water with a calculated γ_{lv} value of 93 mJ/m^2 instead of an experimental value of 72.8 mJ/m^2. Considering the fact that we have only used a simple van der Waals model, the slightly larger deviations for the polar liquids are indeed expected; for example, the Lennard-Jones potential cannot be expected to account for the complicated structure of water.[28]

B. Solid−Liquid Adhesion Patterns. Kwok et al.[3−5] have recently published experimental adhesion and contact angle patterns for a large number of polar and nonpolar liquids on a variety of low-energy solid surfaces, including fluorocarbon FC722, hexatriacontane, cholesteryl acetate, poly(*n*-butyl methacrylate) (P*n*-BMA), poly(methyl methacrylate/*n*-butyl methacrylate), and poly(methyl methacrylate) (PMMA). We reproduce their results here in Figure 1 and compare them with our patterns calculated from intermolecular potentials. Figure 1a illustrates that, for a given solid surface, say the FC722 surface,

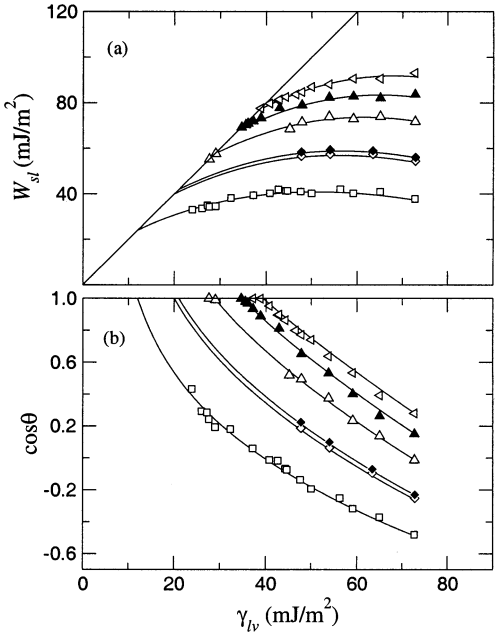

Figure 1. The (a) solid−liquid work of adhesion, W_{sl}, versus the liquid−vapor surface tension, γ_{lv}, and (b) cosine of the contact angle, cos θ, versus the liquid−vapor surface tension, γ_{lv}, for a (□) fluorocarbon FC722, (◇) hexatriacontane, (◆) cholesteryl acetate, (△) poly(*n*-butyl methacrylate), (▲) poly(methyl methacrylate/*n*-butyl methacrylate), and (rotated △) poly(methyl methacrylate) surfaces.

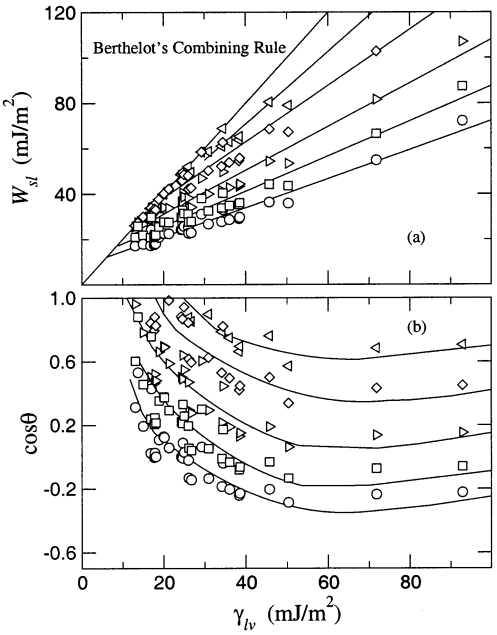

Figure 2. The (a) solid−liquid work of adhesion, W_{sl}, versus the liquid−vapor surface tension, γ_{lv}, and (b) cosine of the contact angle, cos θ, versus the liquid−vapor surface tension, γ_{lv}, calculated from the Berthelot combining rule, eq 2.

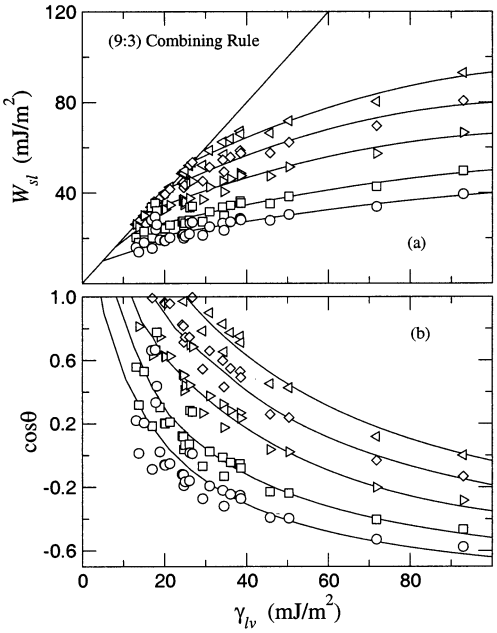

Figure 3. The (a) solid−liquid work of adhesion, W_{sl}, versus the liquid−vapor surface tension, γ_{lv}, and (b) cosine of the contact angle, cos θ, versus the liquid−vapor surface tension, γ_{lv}, calculated from the (9:3) combining rule, eq 11.

the experimental solid−liquid work of adhesion, W_{sl}, increases as γ_{lv} increases up to a maximum W_{sl} value identified as W_{sl}^*. Further increase in γ_{lv} causes W_{sl} to decrease from W_{sl}^*. The trend described here appears to shift systematically to the upper right for a more hydrophilic surface (such as PMMA) and to the lower left for a relatively more hydrophobic surface. There are also some indications that the location of the maximum point, W_{sl}^* appears to shift to the right as surface hydrophobicity decreases. Figure 1b shows the experimental contact angle patterns in cos θ versus γ_{lv}. We see that, for a given solid surface, as γ_{lv} decreases, cosine of the contact angle (cos θ) increases, intercepting at cos $\theta = 1$ with a "limiting" γ_{lv} value. We identify this "limiting" value as γ_{lv}^c. As γ_{lv} decreases beyond this γ_{lv}^c value, contact angles become more or less zero (cos $\theta \approx 1$), representing the case of complete wetting. The trend described here appears to change systematically to the right for a more hydrophilic surface (such as PMMA) and to the left for a relatively more hydrophobic surface (such as fluorocarbon). Changing the solid surfaces in this manner changes the limiting γ_{lv}^c value, suggesting that γ_{lv}^c might be of indicative value as a solid property. In fact, Zisman labeled this γ_{lv}^c value as the critical surface tension of the solid surface, γ_c.[29−31]

1. Berthelot's Rule. The 30 liquids in Table 1 were used to calculate the solid−vapor and solid−liquid surface tensions for the adhesion patterns using Berthelot's, (9:3), Steele's, and (12:6) combining rules. Our calculation results suggest that Berthelot's rule is the worst among all combining rules that we have considered here, and the results are shown in Figure 2. The calculated adhesion and contact angle patterns do not follow the general patterns shown in Figure 1. In fact, the discrepancies are quite large that Berthelot's rule predicts cosine of the contact angle to increase with larger γ_{lv}, contrary to the experimental patterns. The fact that Berthelot's rule could not give a reasonable prediction is well-known because it generally overestimates the strength of unlike interactions from like pairs.[23]

2. (9:3) Combining Rule. The calculated adhesion and contact angle patterns for the (9:3) combining rule are shown in Figure 3. In Figure 3a, the (9:3) combining rule reasonably predicts the general trend of the adhesion patterns: increasing γ_{lv} increases W_{sl} monotonically. It is not apparent, however, that there exists a maximum W_{sl}^* beyond which W_{sl} will decrease when γ_{lv} increases, as in Figure 1. The general adhesion pattern predicted from the (9:3) combining rule is that W_{sl} increases with γ_{lv}. To change the hydrophilicity of the model surface and observe the change in patterns, we hypothesize that solid surface

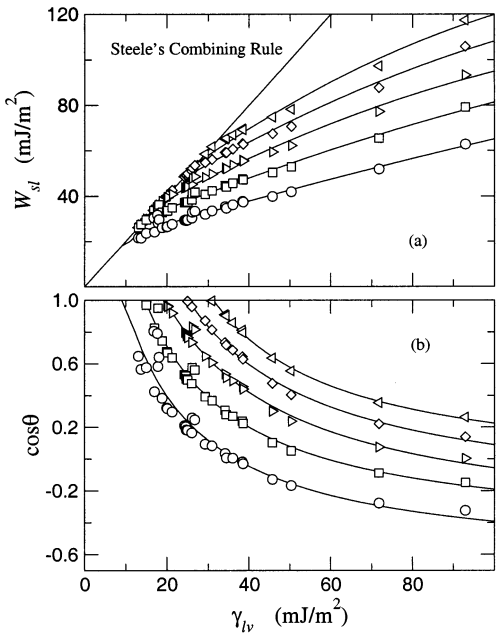

Figure 4. The (a) solid−liquid work of adhesion, W_{sl}, versus the liquid−vapor surface tension, γ_{lv}, and (b) cosine of the contact angle, cos θ, versus the liquid−vapor surface tension, γ_{lv}, calculated from the Steele combining rule, eq 13.

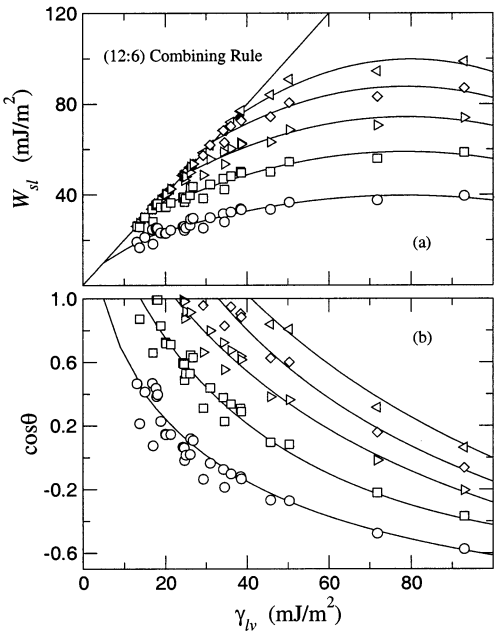

Figure 5. The (a) solid−liquid work of adhesion, W_{sl}, versus the liquid−vapor surface tension, γ_{lv}, and (b) cosine of the contact angle, cos θ, versus the liquid−vapor surface tension, γ_{lv}, calculated from the (12:6) combining rule, eq 15.

energy increases with stronger solid−solid interaction energy, ϵ_{ss}; increasing the solid−solid interactions increases the surface free energy required to generate a unit interfacial surface area. Thus, we increased the solid−solid interactions systematically to model hydrophilic surfaces and decreased the interactions for hydrophobic ones. Increasing the interactions and, hence, the surface hydrophilicity shifts the curves in Figure 3a to the upper right, in good agreement with those from Figure 1a. Figure 3b illustrates the calculated contact angle patterns: decreasing γ_{lv} increases cos θ for a given solid surface. Further decrease in γ_{lv} causes cos θ to intercept at cos $\theta = 1$ with $\gamma_{lv} = \gamma_{lv}^{c}$, identifying the case of complete wetting. Increasing the hydrophilicity of the surface shifts the curves in Figure 3b to the right, similar to those shown in Figure 1b. We also note the relatively larger scatters in Figure 3; it will become apparent later that the magnitude of such scatters depends on the choice of the combining rules.

3. Steele's Combining Rule. The adhesion and contact angle patterns calculated from Steele's combining rule are shown in Figure 4. It appears that Steele's combining rule also predicts the general adhesion and contact angle patterns well, in good agreement with the experimental results shown in Figure 1. We note that this combining rule yields results that have significantly less scatters than those calculated from the (9:3) combining rule (in Figure 3). However, the calculated results for W_{sl} in Figure 4a still increase monotonically with increasing γ_{lv} and did not result in a maximum W_{sl}^{*} value that was observed in the experimental results in Figure 1.

4. (12:6) Combining Rule. The calculated results using the (12:6) combining rule are shown in Figure 5. In Figure 5a, we see that the (12:6) combining rule appears to predict correctly the existence of a maximum W_{sl}^{*} value as γ_{lv} increases. This maximum value was not observed using the (9:3) and Steele's combining rules in Figures 3 and 4, respectively. The calculated contact angle patterns in Figure 5b are also similar to those from the (9:3) and Steele's combining rules and in good agreement with the patterns observed experimentally. The (12:6) combining rule, however, suffers from the same shortcoming as the (9:3) combining rule in which relatively larger scatters were apparent.

We conclude that the adhesion and contact angle patterns observed experimentally can, in principle, be reproduced from considerations of only intermolecular forces. The accuracy of the prediction depends on the choice of the combining rule and intermolecular potentials used. The Steele combining rule produces less scatters; the (12:6) combining rule correctly predicts the maximum solid−liquid adhesion work that was observed from experimental results.

IV. Summary

We have examined the patterns of adhesion and contact angles calculated from several commonly used combining rules in conjunction with intermolecular potentials using a mean-field approximation. Results suggested that, on one and the same solid surface, the free energy of solid−liquid adhesion, W_{sl}, increases with γ_{lv} until it reaches a maximum W_{sl}^{*} value. Further increase in γ_{lv} causes W_{sl} to decrease from this maximum W_{sl}^{*}. Changing from a hydrophobic surface to a more hydrophilic one shifts the curves regularly to the upper right. The regularity of the patterns is remarkable. We also found that cosine of the contact angles, cos θ, for different liquids on one and the same solid surface increases as the liquid−vapor surface tension, γ_{lv}, decreases, intercepting at cos $\theta = 1$ at $\gamma_{lv} = \gamma_{lv}^{c}$. Increasing the hydrophilicity shifts the curves regularly to the right. Except the Berthelot rule, the (9:3), Steele's, and (12:6) combining rules studied here are capable of predicting the general patterns of adhesion and contact angle that was observed from experiments. The combining rule from Steele produces more satisfactory results with less scatters; the (12:6) combining rule yields a maximum work of solid−liquid adhesion, similar to those observed from experimental results. Macroscopic experimental adhesion and contact angle patterns can, in principle, be reproduced qualitatively from consideration of only intermolecular forces. The exact patterns would depend on the choice of the combining rules, which might not necessarily give good results.

Acknowledgment. We gratefully acknowledge financial support from the Alberta Ingenuity Establishment Fund, Canada Research Chair (CRC) Program, Canada Foundation for Innovation (CFI), Petro-Canada Young Innovator Research Fund, and Natural Science and Engineering Research Council of Canada (NSERC) in partial support of this research. J.F. acknowledges financial support from the Alberta Ingenuity in the form of a studentship. We also acknowledge a program and helpful discussion from Dr. A. E. van Giessen.

References and Notes

(1) Kwok, D. Y.; Gietzelt, T.; Grundke, K.; Jacobasch, H. J.; Neumann, A. W. *Langmuir* **1997**, *13*, 2880.
(2) Kwok, D. Y.; Lin, R.; Mui, M.; Neumann, A. W. *Colloids Surf., A* **1996**, *116*, 63.
(3) Kwok, D. Y.; Neumann, A. W. *J. Phys. Chem. B* **2000**, *104* (4), 741.
(4) Kwok, D. Y.; Ng, H.; Neumann, A. W. *J. Colloid Interface Sci.* **2000**, *225* (2), 323.
(5) Kwok, D. Y.; Neumann, A. W. *Adv. Colloid Interface Sci.* **1999**, *81*, 167.
(6) Reed, T. M. *J. Phys. Chem.* **1955**, *59* (5), 425.
(7) Reed, T. M. *J. Phys. Chem.* **1955**, *59* (5), 428.
(8) Hudson, G. H.; McCoubrey, J. C. *Trans. Faraday Soc.* **1960**, *56*, 761.
(9) Fender, B. E. F.; Halsey, G. D., Jr. *J. Chem. Phys.* **1962**, *36*, 1881.
(10) Sullivan, D. E. *Phys. Rev. B* **1979**, *20* (10), 3991.
(11) Sullivan, D. E. *J. Chem. Phys.* **1981**, *74* (4), 2604.
(12) Matyushov, D. V.; Schmid, R. *J. Chem. Phys.* **1996**, *104* (21), 8627.
(13) Rowlinson, J. S.; Swinton, F. L. *Liquids and Liquid Mixtures*; Butterworth Scientific: London, 1981.
(14) Chao, K. C.; Robinson, J. R. L. *Equation of State: Theories and Applications*; American Chemical Society: Washington, DC, 1986.
(15) Steele, W. A. *The Interaction of Gases with Solid Surfaces*; Pergamon Press: New York, 1974.
(16) Berthelot, D. *C. R. Hebd. Seances Acad. Sci.* **1898**, *126* (1703), 1857.
(17) Israelachvili, J. N. *Proc. R. Soc. London, Ser. A* **1972**, *331*, 39.
(18) Kestin, J.; Mason, E. A. *AIP Conf. Proc.* **1973**, *11*, 137.
(19) Steele, W. A. *Surf. Sci.* **1973**, *36*, 317.
(20) Lane, J. E.; Spurling, T. H. *Aust. J. Chem.* **1976**, *29*, 8627.
(21) Dupré, A. *Théorie Mécanique de la Chaleur*; Gauthier-Villars: Paris, 1969.
(22) Good, R. J.; Elbing, E. *Ind. Eng. Chem.* **1970**, *62* (3), 72.
(23) Maitland, G. C.; Rigby, M.; Smith, E. B.; Wakeham, W. A. *Intermolecular Forces: Their Origin and Determination*; Clarendon Press: Oxford, U.K., 1981.
(24) Girifalco, L. A.; Good, R. J. *J. Phys. Chem.* **1957**, *61*, 904.
(25) van Giessen, A. E.; Bukman, D. J.; Widom, B. *J. Colloid Interface Sci.* **1997**, *192*, 257.
(26) Carnahan, N. F.; Starling, K. E. *Phys. Rev. A* **1970**, *1* (6), 1672.
(27) Jaspers, J. J. *J. Phys. Chem. Ref. Data* **1972**, *1*, 841.
(28) Yang, B.; Sullivan, D. E.; Gray, C. G. *J. Phys.: Condens. Matter* **1994**, *6*, 4823.
(29) Fox, H. W.; Zisman, W. A. *J. Colloid Sci.* **1952**, *7*, 428.
(30) Hare, E. F.; Shafrin, E. G.; Zisman, W. A. *J. Phys. Chem.* **1954**, *58*, 236.
(31) Zisman, W. A. In *Contact angle, wettability and adhesion*; Gould, R. F., Ed.; Advances in Chemistry Series 43; American Chemical Society: Washington, DC, 1964.